UNCLASSIFIED

AD **273 630**

Reproduced
by the

ARMED SERVICES TECHNICAL INFORMATION AGENCY
ARLINGTON HALL STATION
ARLINGTON 12, VIRGINIA

UNCLASSIFIED

OPTICAL CALIBRATION OF THE U.S. NAVAL SPACE SURVEILLANCE SYSTEM

L. O. Hayden

Space Surveillance Branch
Applications Research Division

March 14, 1962

NOX

U. S. NAVAL RESEARCH LABORATORY
Washington, D.C.

CONTENTS

ABSTRACT

A project was initiated in the Spring of 1960 to calibrate the Space Surveillance System by means of ballistic cameras. The principle behind this calibration is a comparison between the positions of the Echo balloon as determined by radio-frequency reflections of the Space Surveillance System and as determined by photographs against a star background. The preliminary results show that all stations have zero errors of l e s s than 0.1 degree at the zenith. A second error having a standard deviation of about 0.05 degree is due in part to the limited precision of measurement used. The report describes the work done prior to the second phase of calibration, that phase leading to a much higher precision.

PROBLEM STATUS

This is an interim report on the first phase of c a l i b r a t i o n; work is continuing.

AUTHORIZATION

OPTICAL CALIBRATION OF THE U.S. NAVAL SPACE
SURVEILLANCE SYSTEM

INTRODUCTION

The U.S. Naval Space Surveillance System contains four radio interferometer-type receiving stations located along a great circle which crosses the southern part of the United States. The receiving stations are located at Ft. Stewart, Georgia; Silver Lake, Mississippi; Elephant Butte, New Mexico; and Brown Field, Chula Vista, California. Three transmitters are located at suitable points remote from the receiving stations along the same great circle. These transmitters provide sources of electromagnetic radiation which induce secondary radiation from satellites when they enter the fields generated by the transmitting stations.

The transmitting and receiving antennas form fan-shaped patterns along the plane of the great circle, so that the region of detection is confined approximately to this plane. Hence, an angular measurement of the direction to a satellite taken simultaneously from each of two receiving stations is sufficient to determine the three position coordinates of the satellite at the time of measurement. The purpose of optical calibration is to determine any small errors existing in the angular measurements obtained with the interferometer, and thus improve the accuracy of the system. Since the far field of the antennas is higher than conventional aircraft fly, the method chosen uses photographs of the Echo balloon against a star background. Simultaneous radio-frequency reflection from the satellite permits the system to be calibrated.

In anticipation of the launching of the Echo satellite, a project to calibrate the Space Surveillance System by optical means was assigned in April 1960. A minimum accuracy of measurement of 0.1 degree was considered sufficient to provide useful calibration data and was adopted as an initial goal. To carry out the project it was necessary to acquire and install suitable cameras at each receiving station, and to provide these cameras with time coding equipment. Also, a reduction procedure was necessary to obtain the position of the satellite with respect to the receiving station as a function of time, as the angle so determined optically would be compared with the angle measurement taken from the interferometer to obtain the calibration error.

INSTRUMENTATION

At the time this project was initiated a camera employing a "K38" f/6.3 lens with a 24-inch focal length and an equatorial mount with sidereal drive was available at the NRL Chesapeake Bay Annex. Time coding equipment devised by E. Habib of NASA was used with this camera. Habib's method involved displacing the photographic plate with a solenoid actuated plunger. After making initial tests on this camera, the entire assembly was shipped to the Ft. Stewart, Georgia, Space Surveillance Station and put into operation in October 1960. Figure 1 shows a photograph taken with this camera.

The breaks in the satellite trail produced by the time coding are clearly visible on the trail of the satellite. The time code marks appear at 2-second intervals except during the readout of Universal Time, which starts exactly on each minute. The digital time code is formed by pulses separated by 1/5 second. Four bursts of pulses appear at 2-second intervals to give the four digits required to read the time of day on a 24-hour clock. As
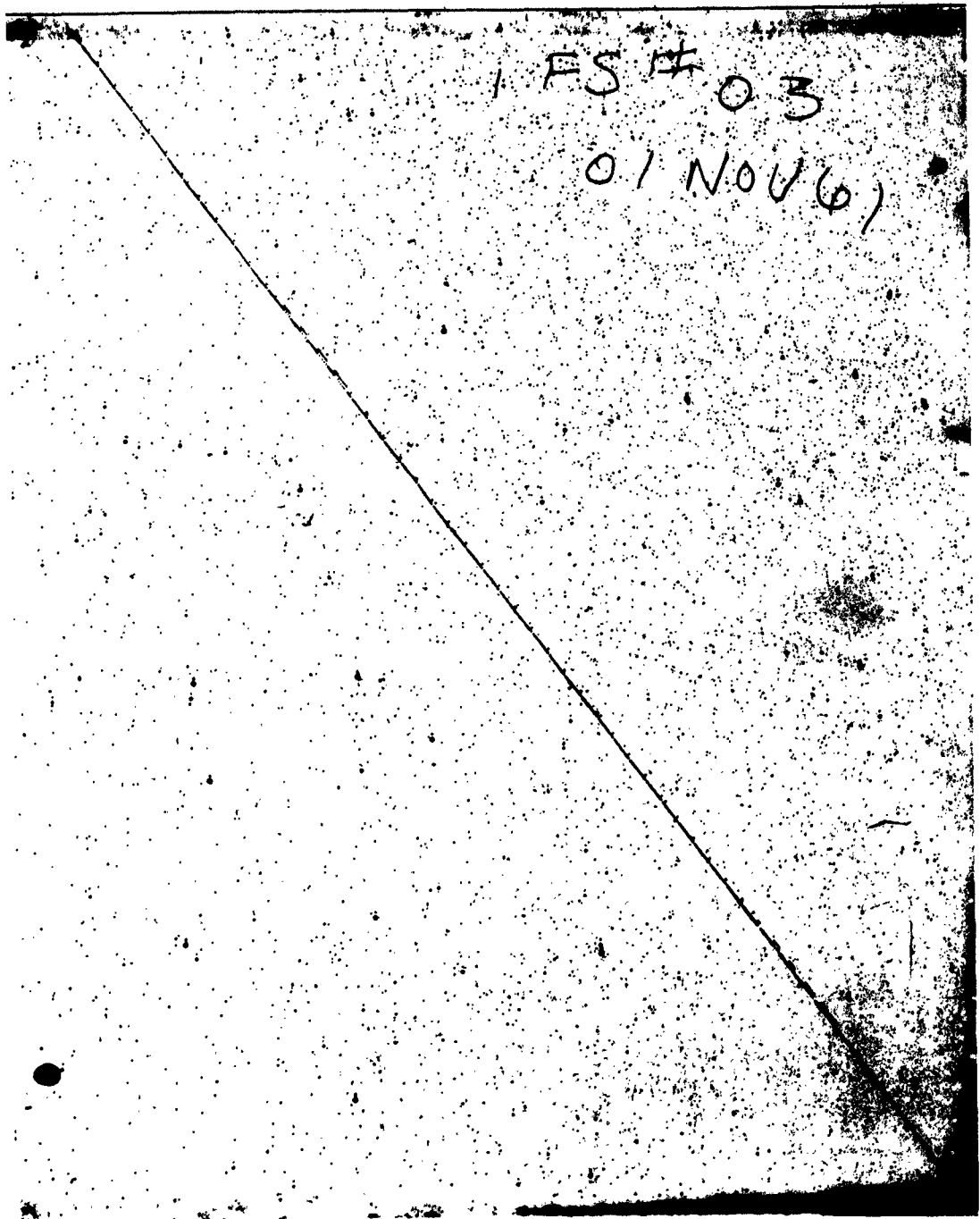
Fig. 1 - Trail of the Echo satellite photographed at Ft. Stewart, Georgia. The time coding was done by displacing the photographic plate, producing notches in the trail.

a consequence of the plate displacement during exposure, the stars have double images. The displaced images are much fainter because of the relatively small exposure time and cause no problem in plate reduction.

A small plywood box camera loaned by Norton Goodwin of the Volunteer Satellite Tracking Program was set up at Silver Lake, Mississippi. It employed an f/2.5 Aero Ektar lens with a 7-inch focal length. Despite apparent crude construction of this camera, its optical quality was excellent. This camera was used to obtain trail type images. Breaking of the satellite trail was done manually with a mask, a method used to some extent by amateur satellite photographers. This camera provided useful data as early as September 12, 1960, at the Silver Lake site.

Construction of three additional equatorial mounts of the type used at Ft. Stewart, Georgia was begun in the Fall of 1960. The new mounts were equipped with K37-type aircraft cameras. The shutter actuation mechanism in these cameras was so designed that the shutters could be opened by the application of 28 volts dc. To utilize this built-in capability a notched disc was fabricated and mounted on a 1-rpm synchronous motor shaft. The notches alternately opened and closed a microswitch in the 28-volt line to the shutter drive mechanism. This voltage was also fed to a multichannel recorder and displayed with Universal Time and other information. Identifying notches were inserted at 120-degree intervals around the notched disc, making each 20-second interval unique within a 1-minute interval. Since auxiliary information taken from the interferometer records defines the time at which the satellite crossed the antenna beam, no problem of identifying the minute interval exists. Figure 2 is an example of the type of time coding obtained by this method.

Figure 3 is a sample of recorded data which gives the phase information from which the zenith angle of the satellite is determined. Along the lower margins appears the coded Universal Time. Directly above the time the agc response is shown as the satellite crossed the plane of the great circle usually referred to as the "fence." In the next channel is a record of the voltage applied to the shutter drive mechanism. This is used in determining the Universal Time for points along a satellite trail such as the one shown in Fig. 2. The installation of the three additional cameras at the receiving sites was completed in May 1961.

DATA REDUCTION

The modest requirement of 0.1-degree accuracy in angle determination allowed some choice of method in reducing photographic plates. The method used is essentially as follows: A star chart photographed to the same scale as the plates to be reduced is placed over an illuminated viewer. The photographic plate to be reduced is placed over the star chart and adjusted to match the stars on the chart. The path of the satellite trail among the stars is carefully observed and plotted on the chart. Time information may also be designated along the satellite trail by reference to the photographic plate. Figure 4 is a plot of such a satellite trail. It is also necessary to find the projection among the stars of the fence. Since the celestial coordinates are based on the position of the vernal equinox, there is a slow but continual drift of the coordinate grid among the stars. To compensate for this the present-day celestial coordinates of the fence are transformed to the set used in preparing the star chart. (In the case of the Bonner Durchmusterung the Epoch date for the chart coordinates is 1855.) The information on the fence coordinates is plotted in the neighborhood of the satellite trail which intersects it. One degree intervals are marked along the line representing the fence in Fig. 4. The displacement of the time of fence crossing indicated by the interferometer system from that obtained by the optical system has been too small to be considered in the method described above. On the other hand the differences in the optically measured zenith angles and the angles obtained from the interferometer have been quite appreciable. It is this zenith angle error which has been investigated in some detail. Measurements of optical zenith angle are read to 0.01 degree from the chart. This graphical procedure has little of the elegance of the method using an optical
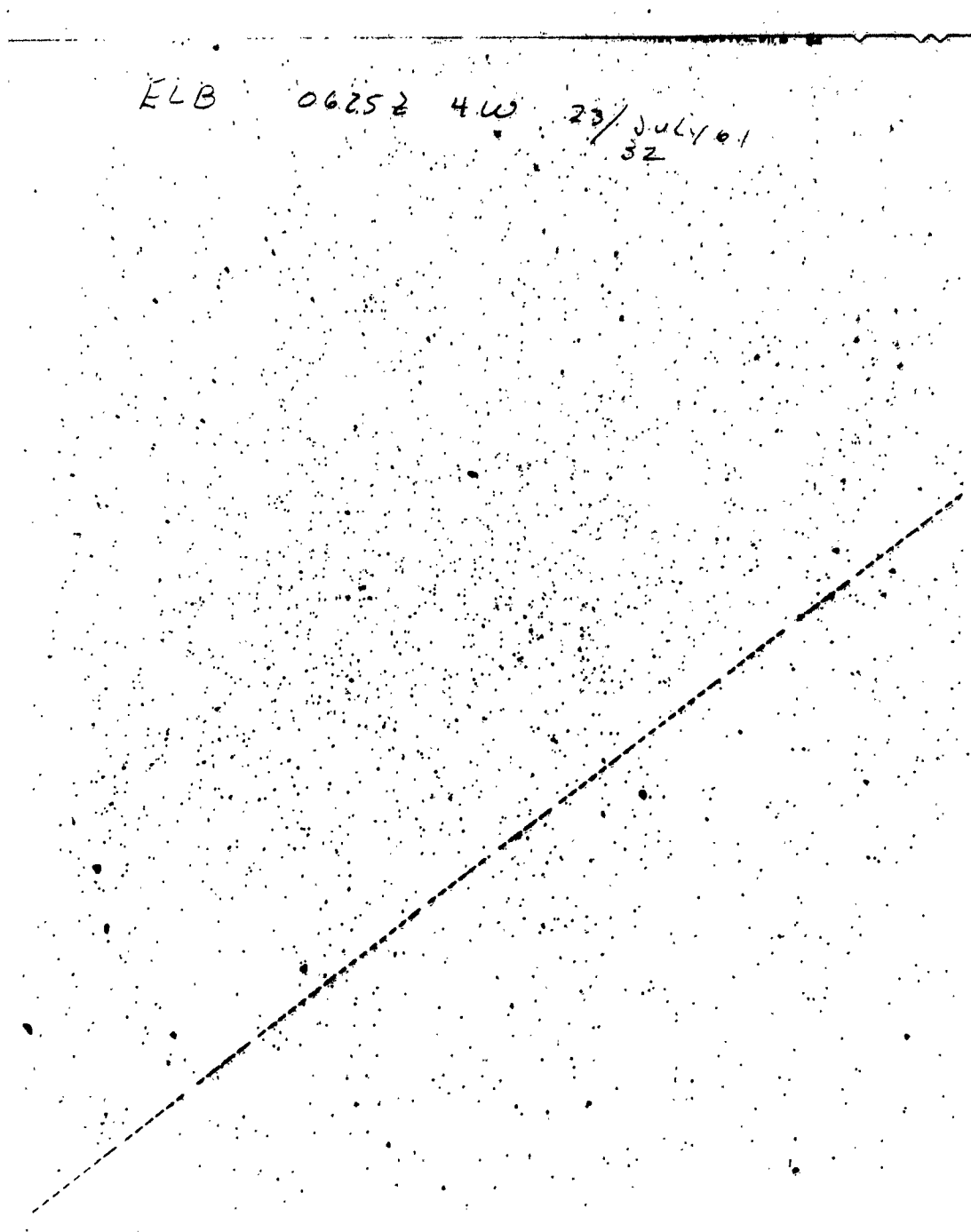
Fig. 2 - Example of an Echo satellite trail showing time coding
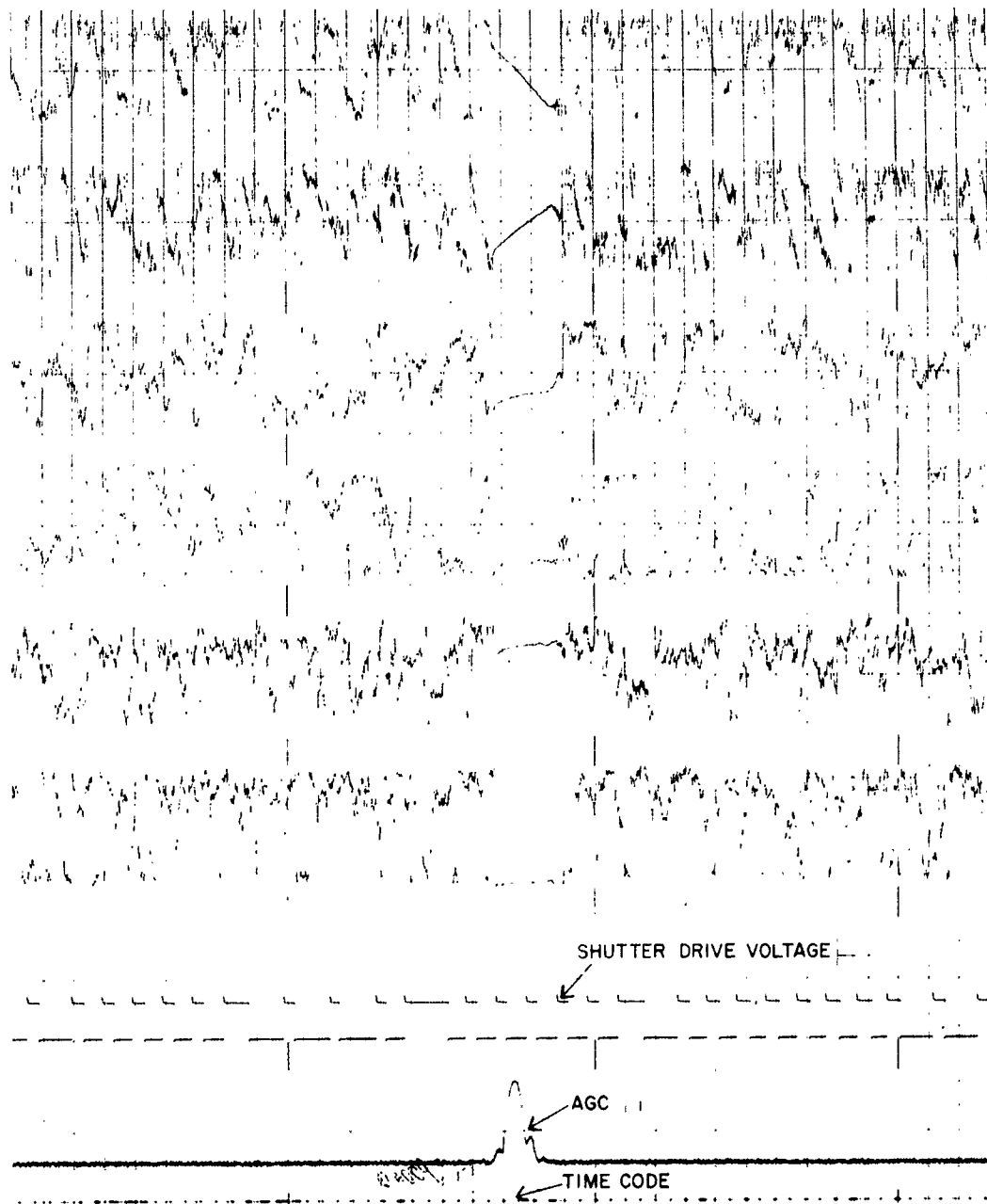produced by an electrically actuated shutter mechanism

SHUTTER DRIVE VOLTAGE

AGC

TIME CODE

Fig. 3 - Sample of the recorded data from which the zenith angle
of the satellite is determined

STATION: FORT STEWART
DATE MARCH 11, 1961

ANGLE OF CROSSOVER
14.15° EAST

0038000.0 UT

FENCE

EAST

TIME OF CROSSOVER
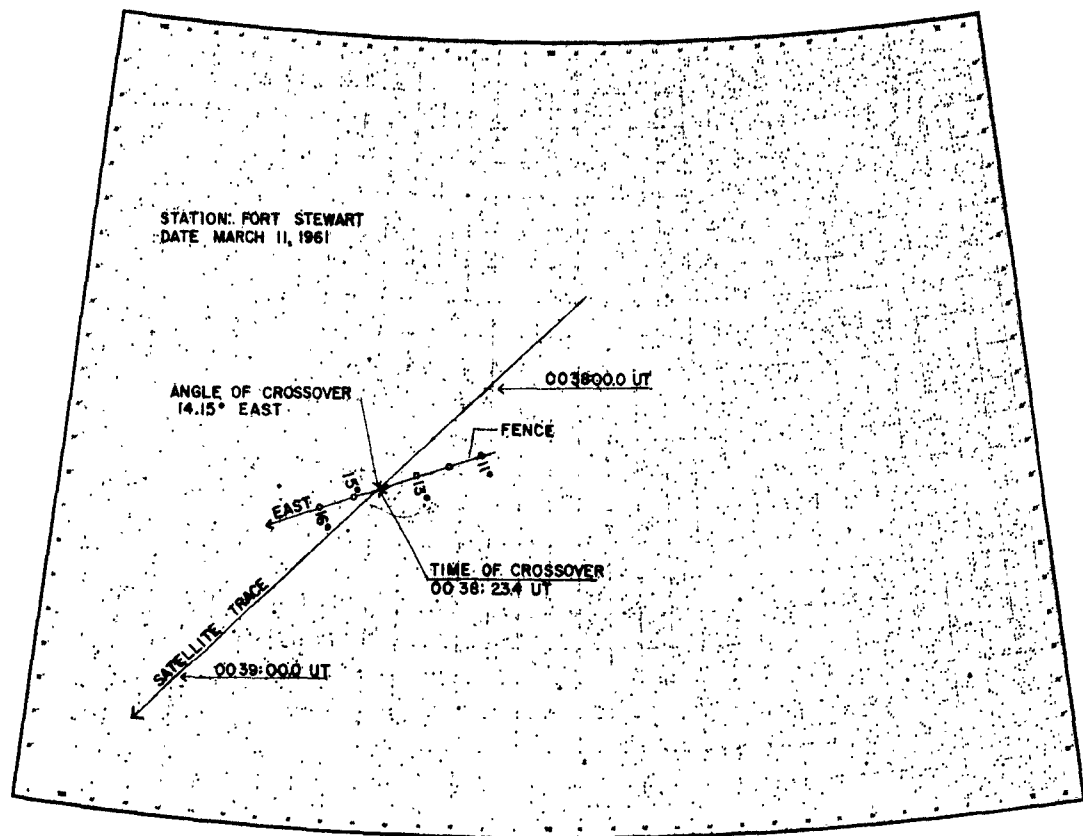00 38: 23.4 UT

SATELLITE TRACE

0039:00.0 UT

Fig. 4 - Satellite trail and fence projection superimposed on a star chart

comparator; but neither does it require as much time to obtain reasonably good information. It has been estimated that the overall zenith angle measurement error is about 0.05 degree. This error is attributed largely to plotting and reading of the graph. The data reduced by this method, which is treated below, verifies that this is a reasonable estimate of the error of this method.

ANALYTICAL METHODS

It has been indicated above that only the zenith angle error is of consequence. The remainder of this report is concerned with comparing the zenith angle obtained by optical methods with angle measurements taken from the interferometers and the data transmission system. Figure 5 presents a block diagram of one pair of antennas used in the radio interferometer and traces the signal from the receiving site to the data processing center at the Naval Weapons Laboratory, Dahlgren, Virginia, where the phase information from the antenna pair appears on one channel of a multichannel recording similar to the one shown in Fig. 3. The phase data recorded at NWL has been reduced at NRL, using in part, calibration data readings made at NWL. A summary of the reduction of these data, is given in Tables 1-4 at the end of the report. (The details of these tables will be discussed later in the report.) A second source of data has been the records taken at the receiving sites, which is in part a duplication of the NWL data.
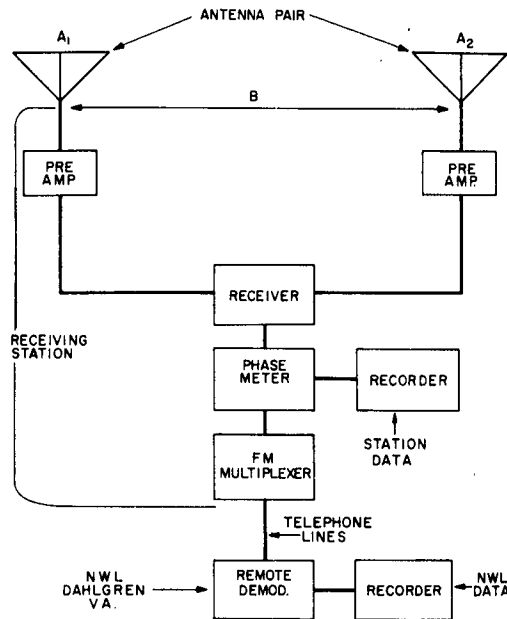
Fig. 5 - The processing of the signal
from one pair of antennas

By comparing the phase data taken at these two points in the system, it has been possible to look for any degradation in the phase information during its transmission to the remote data center at NWL. The two sources of recorded data also provided a check on time coding and possible errors in the reduction. The angle information obtained from the two sources has been compared with optical measurements.

In making this comparison, it was found desirable to depart slightly from the customary angle designation used in Space Surveillance. Customarily the direction of arrival of a signal from a satellite is described as θ degrees east or θ degrees west of zenith according to the case. This is equivalent to using spherical coordinates in which the zenith angle θ plays the conventional role and ϕ takes one of two values separated by 180 degrees. It was much more convenient for this analysis to use a single coordinate as shown in Fig. 6.
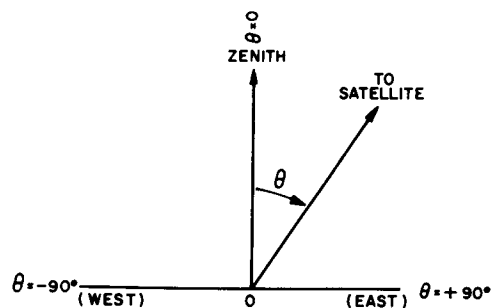

Fig. 6 - Single-angle coordinate ranging
from -90 to +90 degrees

This was done by assigning a positive value to zenith angles in the east and a negative value to those in the west.* By doing this θ as well as $\sin \theta$ are continuous single-valued functions throughout the region of interest.

Perhaps the most natural form in which to present errors in the interferometer angle measurement is in terms of angle error as a function of zenith angle. This has been done by plotting the difference function

$$\Delta\theta_1 \equiv \theta_r - \theta_o \tag{1}$$

for Ft. Stewart, Georgia, in Fig. 7(a) and for Silver Lake, Mississippi, in Fig. 7(b), with θ_r being defined as the angle measured by the interferometer and θ_o that determined by optical instruments.

In Fig. 7(a) it is seen that a marked increase in angular error takes place for zenith angles beyond -70 degrees in the west. A curve having the best fit passed through the distribution of points may be used to obtain a mean value of error in the interferometer data as a function of zenith angle. This procedure, although mathematically valid provides no insight into the cause of the error and fails to provide a firm basis for projecting the curve over angles for which no optical observations have been made. Figure 7(b) presents a more severe condition which would be difficult to resolve without resorting to a more powerful method of analysis. To continue the analysis, one seeks an analytical expression for a curve that will fit the observed points of Fig. 7(a), or, what is equivalent, a transformation in which the curve through the points degenerates to a straight line.

In Fig. 8(a), the data in Fig. 7(a) has been plotted in the form

$$\Delta\sin\theta = \sin\theta_r - \sin\theta_o. \tag{2}$$

It is apparent that the desired straight line has been found. The resulting simple form permits data to be summarized by statistical averaging. This has been done for all baselines and the results are given in Tables 1-4. The error in the sine of the zenith angle is independent of the zenith angle within the limits of the accuracy of the equipment used for making optical measurements. Since the dependence on angle of arrival was removed by the transformation to sine functions, it is useful to replace the zenith angle by time as a plotting parameter, as the possibility of calibration changes over long periods of time is one of the questions for which an answer has been sought. Accordingly the plot for Silver Lake is presented as a function of time in Fig. 8(b).

The time dependent plot reduces the confusion of Fig. 7(b) to order. It is apparent that a new factor entered the measurements at Silver Lake. A change in the calibration error appears to have taken place between January 10 and 12, 1961. (A second shift in calibration was introduced between 1800 and 2020Z June 28, 1961, to correct the condition which existed during the previous months.) To explain the nature of the error which has been found in the graphs, let us refer to the basic geometry of the system. In Fig. 9 is shown a pair of antenna arrays A_1 and A_2 separated by a distance B. θ is the angle between the zenith and the direction of arrival of a signal. It is clear that

$$\sin\theta = \frac{S}{B} = \frac{n + \phi}{B} \tag{3}$$

---

*The choice of signs used here was suggested by an earlier unpublished paper by the author in which θ was defined as the angle between the eastern horizon and the direction of arrival of the signal. The range of θ was $0 \le \theta \le 180°$, and $\cos \theta$ in that treatment had the same value as $\sin \theta$ does here.
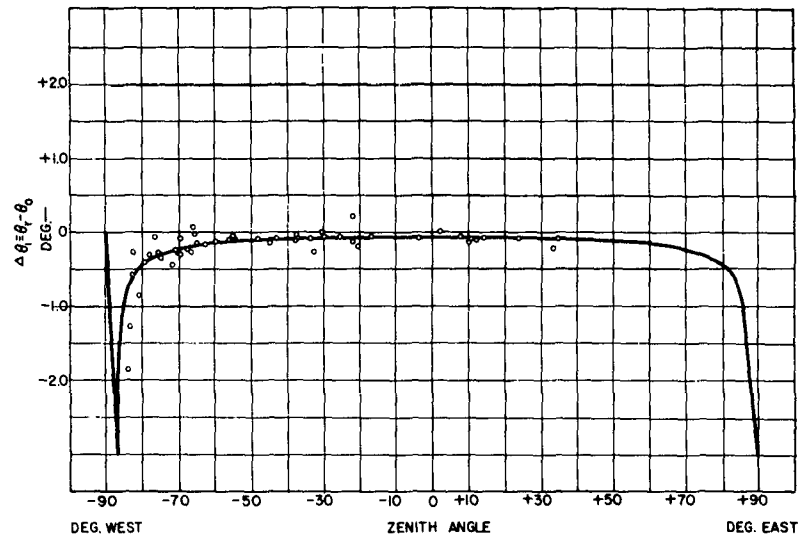
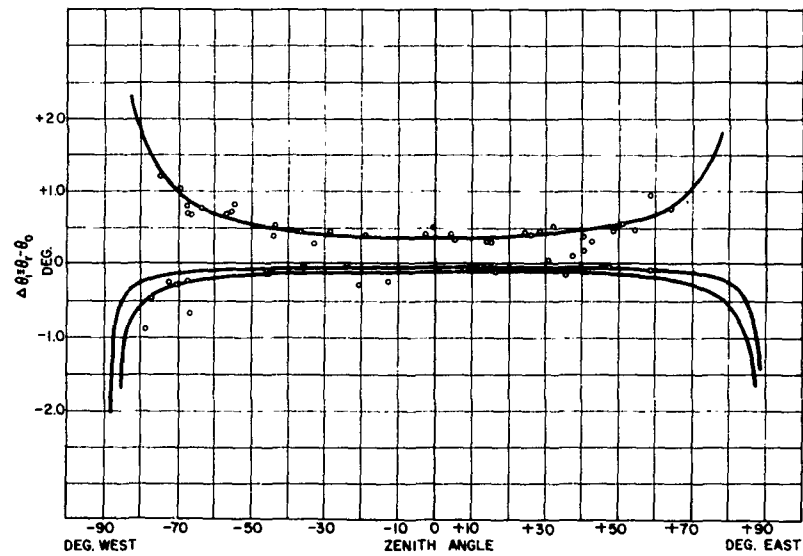Fig. 7(a) - Zenith angle error, Ft. Stewart, Georgia

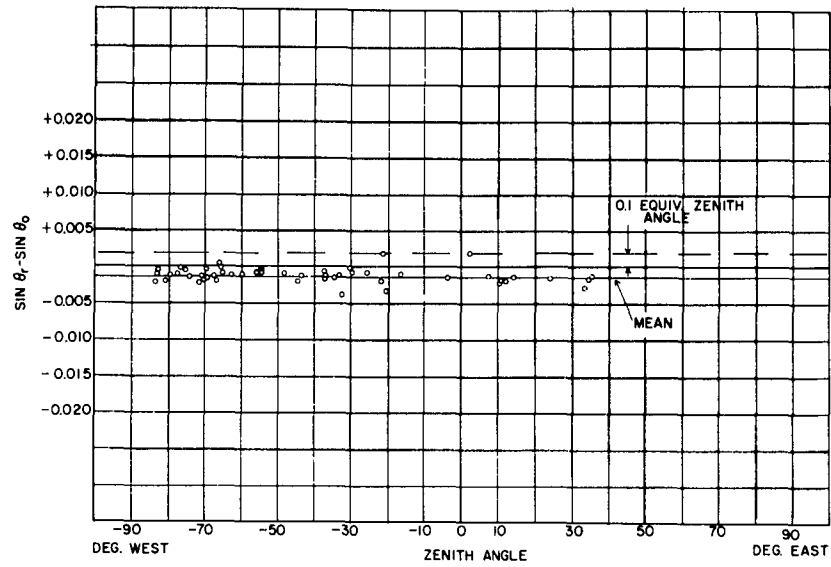Fig. 7(b) - Zenith angle error, Silver Lake, Mississippi

Fig. 8(a) - Data of Fig. 7(a) plotted in the form
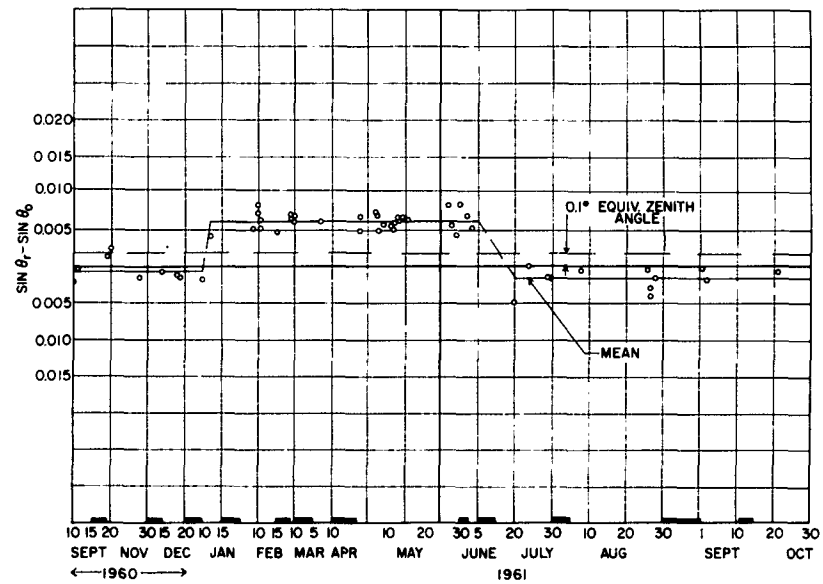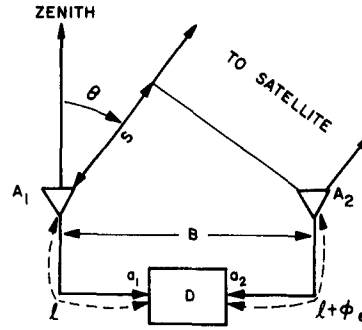of Eq. (2) as a function of zenith angle

Fig. 8(b) - Data of Fig. 7(b) plotted in the form
of Eq. (2) as a function of time

ZENITH

Fig. 9 - Basic geometry of the
system

where n is an integer and ϕ $(0 \le \phi \le 1)$ is the fractional part of a wavelength. Since the phase detector η measures the difference in phase at its inputs a_1 and a_2 rather than the phase equivalent of the distance S, any difference in the phase length ϕ_e of the transmission lines to A_1 and A_2 appears in the output as an additive constant to $n + \phi$. This error converts the theoretical Eq. (3) obtained by geometric considerations into

$$\sin\theta + \Delta\sin\theta = \frac{n + \phi}{B} + \frac{\phi_e}{B} = \frac{m + \Phi}{B} .$$

(4)

A plot of Eq. (3) (solid lines) is given in Fig. 10. It is seen that $(n + \phi)/B$ is a straight line passing through the origin at the zenith and is a composite of the stairstep function n and the sawtooth function ϕ. A second plot in dashed lines has been made for $(m + \Phi)/B$ illustrating the linear relationship between the two functions. It is clear from Fig. 10 and Eq. (4) that the desired phase ϕ may be extracted from the observed phase Φ, provided one knows the value of ϕ_e. From Eqs. (3) and (4) one obtains

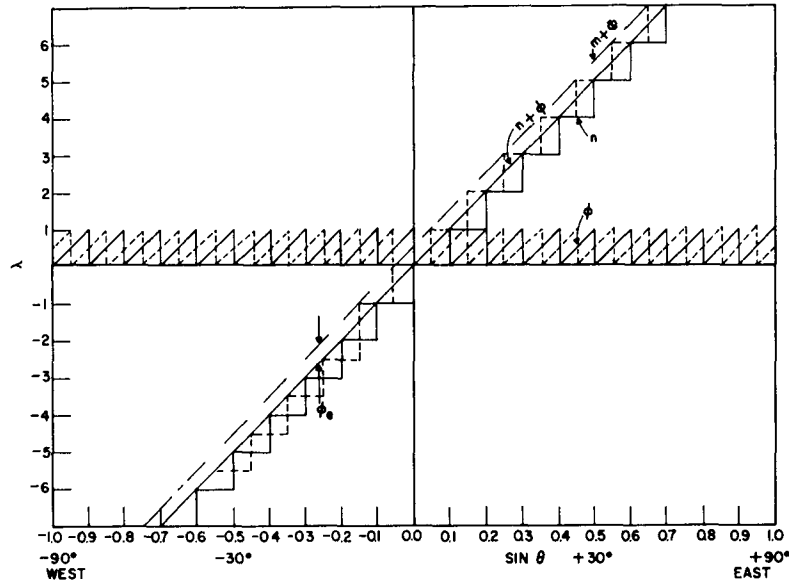$$\phi_e = B \Delta\sin\theta .$$

(5)

Fig. 10 - Plots of Eqs. (3) and (4)

In practice one must recognize that the direction of arrival θ is not measured exactly and that the phase detector may introduce a random phase error. To obtain a more precise value for ϕ_e one must take the mean of a number of observations. Figure 11 shows a plot of the convergence of the mean value of $\Delta\sin\theta$ as a function of the number of measurements, n. On the same graph the function

$$\sigma_m = \frac{\sigma}{\sqrt{n}} \tag{6}$$

has been plotted. σ is obtained from the complete set of observations plotted on the graph. σ_m is taken as an adequate approximation for the probable error in the mean and is included in three proportional forms in Tables 1-4 for maximum convenience for different applications. Because of the small values of probable error in ϕ_e, where an adequate number of observations have been made, it is apparent that this error can be eliminated effectively. This may be done in two ways:

1. ϕ_e may be converted to inches of transmission line and a suitable correction section added (or subtracted) according to the case at a convenient place.

2. $\phi_e \times 100$ is the reading conventionally taken from the recorders; hence $\phi_e \times 100$ may be subtracted from the recorder output readings without making any physical change in the system.

Method 1 has the advantage that once made it requires no further attention. Since a number of weeks is required to recalibrate the system optically, the new calibration constant cannot be checked immediately.

Method 2 is applicable to past data and can be used to study the improvement that results from application to previous analyses. An example of this is illu·trated when the corrections given in Tables 1-4 are applied to the data from Ft. Stewart, Georgia, and Silver Lake, Mississippi. When this is done the angle errors shown in Figs. 7(a) and 7(b) reduce to those shown in Figs. 12(a) and 12(b). In this case the improvement brought about by applying corrections is quite impressive.
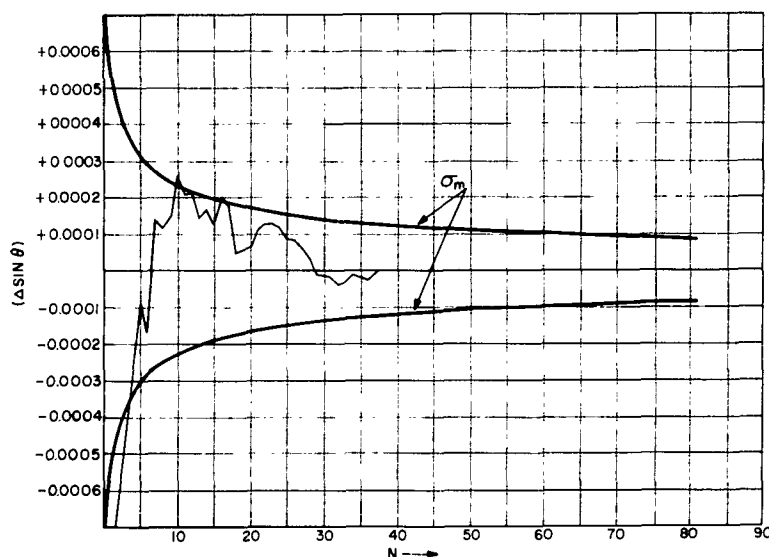

Fig. 11 - Variation of the mean error in sin θ vs the
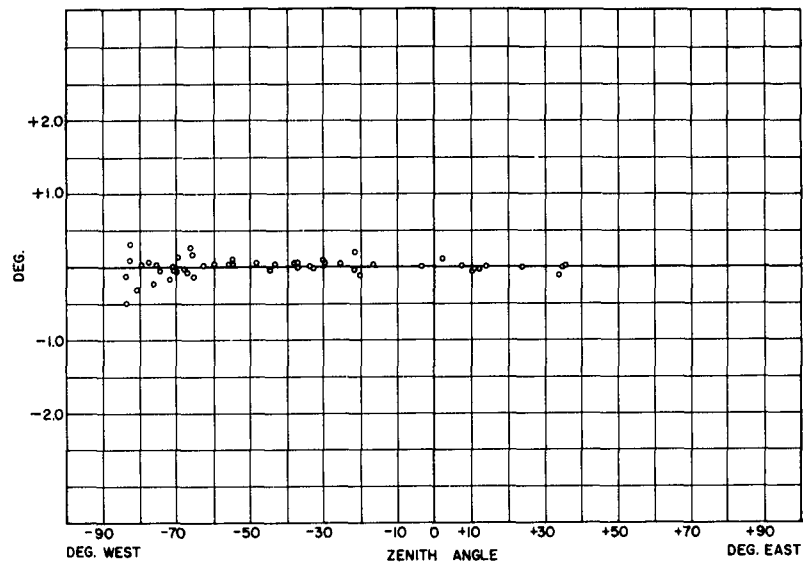number of observations (Ft. Stewart)

Fig. 12(a) - Residual errors in the Ft. Stewart data
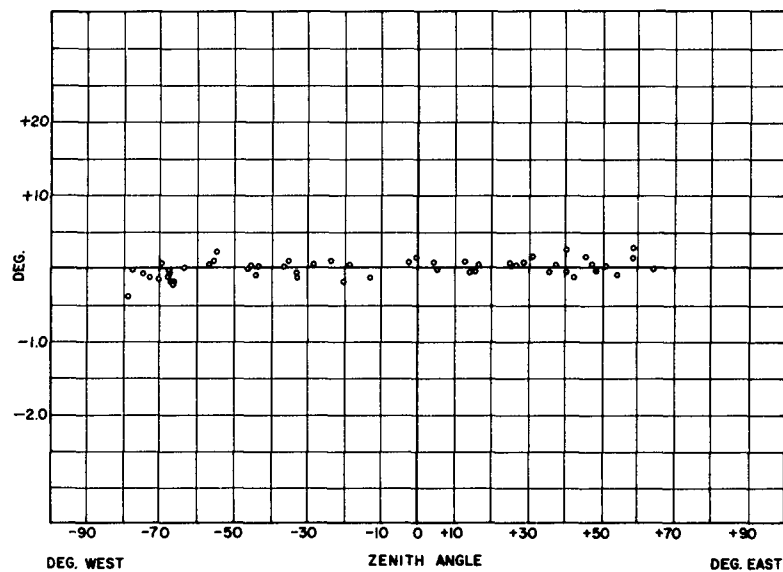of Fig. 7(a) after applying the corrections of Table 1

Fig. 12(b) - Residual errors in the Silver Lake data
of Fig. 7(b) after applying the corrections of Table 2

The standard deviation σ, which measures the probable error of an individual observation, is a more persistent error of the system. However, due to the elaborateness of the system a partial analysis can be made of this variability which leads to additional information on the capability of the system. It is well to proceed by considering some possible causes of the scatter in measurements, which are:

1. Random shifts in the phase measuring equipment and data transmission system.

2. Random errors in reading recording data.

3. Random departures of the direction of arrival of radio signals from the optically observed direction.

4. Random errors in the measurements of optical angles.

These four sources of variations divide into two groups depending on whether the error is in the measurement of ϕ or $\sin \theta$. If one considers the equation

$$\delta\phi = B \; \delta\sin\theta \tag{7}$$

one sees that a variation in $\delta\phi$ due to a variation in $\delta\sin\theta$ approaches zero linearly as B approaches zero. Hence the standard deviation of $\delta\phi$ is independent of variability in the angle error $\delta\sin\theta$ for a sufficiently short baseline. Examination of the values in the tables for $\delta\phi$ shows no trend for baselines not exceeding 136 ft. One is led to assume that the differences in the $\delta\phi$ values for the various baselines results from a choice of samples and variability in quality of different sets of electronics. The average value of the standard deviation of $\delta\phi$ for NWL data for all these baselines is 0.0394λ. Using this value one may derive a capability limit of the system for a given baseline by substituting this value into

$$\delta\sin\theta = \frac{\delta\phi}{B}. \tag{8}$$

Solving this equation indicates that a 520-ft baseline will have an equivalent zenith angle error of 0.04 degree because of internal system variations. Since other random effects may appear as the precision of calibration is extended, it is not known as yet how much the actual random errors will exceed these known limitations due to internal system effects. A larger standard deviation is obtained for the three stations using the 520-ft baselines than is obtained from the shorter baselines at the same stations. Since we have no reason to suspect these baselines to have more noise than the shorter ones, this increase must be attributed to a variation in the measured value of θ due to causes 3 and 4 listed above. Since the relationship of these variations is completely random in respect to the variation (0.0394λ) for phase noise $\delta\phi$, one may extract a value for the variation due to variation in the value of θ by

$$\delta\sin\theta = \sqrt{(\delta\sin\theta)^2_\theta + (\delta\sin\theta)^2_\phi} \tag{9}$$

in which $\delta\sin\theta$ is the standard deviation given under $\Delta\sin\theta$ in the tables, $(\delta\sin\theta)_\phi$ is the contribution to the variability in $\delta\sin\theta$ computed for the noise figure (0.0394λ) in the phase measuring equipment, and $(\delta\sin\theta)_\theta$, which is to be determined, is the variability in the optical measurement of θ. Solution of Eq. (9) gave a value of 0.057 degree for the equivalent zenith angle error due to variations in θ. Since the rise in standard deviation was not evident at Ft. Stewart, where a higher quality optical system is in use, it is believed that this error can be attributed largely to limited capability of the optical

measurements. The value 0.057 degree derived from statistics on the system agrees quite well with the figure 0.05 degree mentioned earlier which was made as an intelligent guess before any of this reduction had been made.

DISCUSSION OF GRAPHS AND TABLES

Some additional details concerning the graphs and tables remain to be discussed. Figures 7(a) and 7(b) give angle error plots for the two stations in the East for which the largest number of observations have been made. A theoretical curve is drawn in Fig. 7(a) which is a transformation of the straight line mean given in Fig. 8(a). The agreement between this curve and observations is quite good. Similar curves are drawn in Fig. 7(b) for the three time-dependent mean-value lines of Fig. 8(b). The zenith angle plot used in Fig. 8(a) has been replaced by a time-dependent plot in Fig. 8(b). To present all of the data for the period on one graph, gaps in the time scale indicated by dark dashes have been inserted. An equivalent zenith angle error of 0.1 degree is also plotted in Figs. 8(a) and 8(b). The equivalent zenith angle is defined as follows:

$$\text{Equiv. zenith angle} = \arcsin |\Delta \sin \theta| .$$

The residual angle errors for Ft. Stewart and Silver Lake were obtained by extracting the proper zero or bias error from the phase readings from these two stations. These plots in Figs. 12(a) and 12(b) are the appropriate form for investigating the effects of refraction. It appears from the data shown here that the measurement of refraction is beyond the capabilities of the data reduction method employed. Graphs for Elephant Butte and San Diego have not been given since all information of interest can be presented more conveniently in tabular form.

The tabulated data have been arranged to give convenient values for various types of applications. $\Delta \sin \theta$ (which is the mean of n observations) and its standard deviation were the first values extracted by the analytical process employed. In Figs. 8(a) and 8(b) the appropriate values of $\Delta \sin \theta$ have been inserted and identified as the mean value for the distributions of points. In the tables the value $\sigma/\sqrt{n}$ is also given as a measure of the probable error in the mean. $\Delta \sin \theta$ is converted to its equivalent in terms of ϕ_e by Eq.(5). This is given in two forms: the first in terms of degrees is convenient for comparison with electrical measurements of line length give results directly in electrical degrees; the second form of ϕ_e is equal to $\lambda \times 100$ so that the error so quoted is equal to percentage error in deflection on the data recorders. The corresponding values $\sigma/\sqrt{n}$ of precision in ϕ_e are given as a confidence factor for the value of ϕ_e. The correction factors for base-lines other than the largest have no effect on the final value of θ, provided they do not cause an error in the value of n of Eq. (3). However they may have a use in connection with data analysis and in setting up automatic angle resolving equipment and accordingly have been included. In some cases definite shifts in calibration have been observed and these have been identified in the tables.

SUMMARY

A preliminary calibration of the Space Surveillance System has met the initial requirement for a precision of 0.1 degree. A bias caused by an error in effective transmission line length has been identified. This can be eliminated by either a mathematical or physical correction to the system. A second type of error is measured in terms of standard deviation. A component of this error has been traced to random internal phase shifts in the interferometer system. A second component due to random variations in the apparent angle of arrival are caused in part by limited precision in the optical reduction procedure. Comparison of data taken from records at the receiving sites and NWL show no significant changes in the data transmission process.

More refined data reduction procedures are being initiated to reduce the errors attributed to the measurements of the optical positions.

Table 1
Ft. Stewart, Georgia, Calibration

Baseline Length (ft)	No. of Obs.	Error Expressed as a Function of $\sin\theta$			Error Expressed as ϕ_e in Terms of Electrical Degrees		Error Expressed as ϕ_e in Terms of Wavelength* (%)		Equiv. Zenith Angle Error (deg)	
		Mean of $\Delta\sin\theta$	Std. Dev., σ ($\delta\sin\theta$)	Probable Error in the Mean, $\sigma/\sqrt{n}$	Mean	Probable Error in Mean, $\sigma/\sqrt{n}$	Mean	Probable Error in Mean, $\sigma/\sqrt{n}$		
413	51	-0.0014	±0.0009	±0.0001	-22.4	±2.2	- 6.2	±0.6	-0.08	±0.05
136	51	-0.0067	±0.0027	±0.0004	-36.2	±2.0	-10.1	±0.6		
52	51	-0.0021	±0.0049	±0.0007	- 4.3	±1.4	- 1.2	±0.4		
28	50	-0.0032	±0.0083	±0.0012	- 3.5	±1.3	- 1.0	±0.3		
24	50	+0.0061	±0.0154	±0.0022	+ 5.8	±2.1	+ 1.6	±0.6		
16	51	-0.0174	±0.0174	±0.0025	-11.0	±1.5	- 3.1	±0.4		

*100% recorder deflection is equal to one wavelength in terms of phase; hence the numbers in this column are equal to the percentage of recorder deflection.

Table 2
Silver Lake, Mississippi, Calibration

Baseline Length (ft)	No. of Obs.	Error Expressed as a Function of $\sin\theta$			Error Expressed as ϕ_e in Terms of Electrical Degrees		Error Expressed as ϕ_e in Terms of Wavelength (%)		Equiv. Zenith Angle Error (deg)	
		Mean of $\Delta\sin\theta$	Std. Dev., σ ($\delta\sin\theta$)	Probable Error in the Mean, $\sigma/\sqrt{n}$	Mean	Probable Error in Mean, $\sigma/\sqrt{n}$	Mean	Probable Error in Mean, $\sigma/\sqrt{n}$		
521*	9	-0.0007	±0.0015	±0.0005	-15.3	±10.1	-4.2	±2.8	-0.04	±0.085
129†	19	+0.0017	±0.0027	±0.0006	+8.6	±3.2	+2.4	±0.9		
60.8	27	+0.0024	±0.0168	±0.0032	+5.9	±7.8	+1.6	±2.2		
52.8	56	+0.0014	±0.0093	±0.0012	+3.2	±2.6	+0.8	±0.7		
20	56	+0.0025	±0.0169	±0.0023	+2.0	±1.8	+0.6	±0.5		
16	56'	-0.0111	±0.0203	±0.0027	-7.0	±1.7	-1.9	±0.5		
521‡	33	+0.0061	±0.0011	±0.0002	+125.2	±4.1	+34.8	±1.1	+0.35	±0.065
129§	37	-0.0013	±0.0017	±0.0003	-6.5	±1.3	-1.8	±0.4		
520¶	12	-0.0017	±0.0015	±0.0004	-35.1	±8.9	-9.7	±2.5	-0.10	±0.085

*Applies from Sept. 12, 1960, to Jan. 10, 1961.
†Applies from Sept. 12, 1960, to Feb. 15, 1961.
‡Applies from Jan. 12, 1961, to June 28, 1961.
§Applies from Mar. 9, 1961, to Oct. 21, 1961.
¶Applies after June 28, 1961.

Table 3
Elephant Butte, New Mexico, Calibration

Baseline Length (ft)	No. of Obs.	Error Expressed as a Function of $\sin\theta$			Error Expressed as ϕ_e in Terms of Electrical Degrees		Error Expressed as ϕ_e in Terms of Wavelength* (%)		Equiv. Zenith Angle Error (deg)	
		Mean of $\Delta\sin\theta$	Std. Dev., σ ($\delta\sin\theta$)	Probable Error in the Mean, $\sigma/\sqrt{n}$	Mean	Probable Error in Mean, $\sigma/\sqrt{n}$	Mean	Probable Error in Mean, $\sigma/\sqrt{n}$		
520	10	-0.0001	±0.0007	±0.0002	-1.0	±4.8	-0.3	±1.3	0.00	±0.04
128	10	+0.0021	±0.0026	±0.0008	+10.7	±4.1	+3.0	±1.1		
60	10	+0.0015	±0.0066	±0.0021	+3.6	±4.9	+1.0	±1.4		
52	10	+0.0041	±0.0088	±0.0028	+8.4	±5.8	+2.3	±1.6		
20	9	+0.0023	±0.0086	±0.0029	+1.8	±2.3	+0.5	±0.6		
16	10	+0.0178	±0.0232	±0.0073	+11.3	±4.6	+3.1	±1.3		

*100% recorder deflection is equal to one wavelength in terms of phase; hence the numbers in this column are equal to the percentage of recorder deflection.

Table 4
San Diego, California, Calibration

Baseline Length (ft)	No. of Obs.	Error Expressed as a Function of $\sin\theta$			Error Expressed as ϕ_e in Terms of Electrical Degrees		Error Expressed as ϕ_e in Terms of Wavelength (%)		Equiv. Zenith Angle Error (deg)	
		Mean of $\Delta\sin\theta$	Std. Dev., σ ($\delta\sin\theta$)	Probable Error in the Mean, $\sigma/\sqrt{n}$	Mean	Probable Error in Mean, $\sigma/\sqrt{n}$	Mean	Probable Error in Mean, $\sigma/\sqrt{n}$		
Applicable from May 11, 1961, to June 3, 1961										
521.8	5	-0.0018	±0.0009	±0.0004	-36.5	±8.3	-10.1	±2.3	-0.10	±0.05
129.6	12	+0.0039	±0.0012	±0.0003	+20.0	±1.8	+5.5	±0.5		
60.8	12	+0.0003	±0.0038	±0.0011	+0.8	±2.6	+0.2	±0.7		
52.8	12	+0.0154	±0.0033	±0.0009	+32.2	±2.0	+8.9	±0.5		
20	12	-0.0115	±0.0155	±0.0045	-9.1	±3.5	-2.5	±1.0		
16	11	-0.0269	±0.0226	±0.0068	-17.0	±4.3	-4.7	±1.2		
Applicable after June 12, 1961										
520	7	+0.0007	±0.0016	±0.0006	+15.0	±12.8	+4.2	±3.5	+0.04	±0.09
128	7	-0.0026	±0.0030	±0.0011	-13.0	±5.8	-3.6	±1.6		
60	7	0.0000	±0.0063	±0.0024	+0.1	±5.7	0.0	±1.6		
52	7	-0.0200	±0.0075	±0.0028	-41.1	±5.8	-11.4	±1.6		
20	6	-0.0206	±0.0164	±0.0067	-16.3	±5.3	-4.5	±1.5		
16	7	+0.0304	±0.0402	±0.0152	+19.3	±9.6	+5.4	±2.7		

UNCLASSIFIED

Naval Research Laboratory. Report 5741.
OPTICAL CALIBRATION OF THE U.S. NAVAL SPACE
SURVEILLANCE SYSTEM, by L.O. Hayden. 18 pp. and
figs., March 14, 1962.

A project was initiated in the Spring of 1960 to
calibrate the Space Surveillance System by means of
ballistic cameras. The principle behind this calibra-
tion is a comparison between the positions of the Echo
balloon as determined by radio-frequency reflections
of the Space Surveillance System and as determined
by photographs against a star background. The pre-
liminary results show that all stations have zero
errors of less than 0.1 degree at the zenith. A second
error having a standard deviation of about 0.05 degree

UNCLASSIFIED   (over)

1. Space surveil-
   lance systems -
   Calibration

I. Hayden, L.O.

UNCLASSIFIED

is due in part to the limited precision of measurement used. The report describes the work done prior to the second phase of calibration, that phase leading to a much higher precision.

UNCLASSIFIED

UNCLASSIFIED

is due in part to the limited precision of measurement used. The report describes the work done prior to the second phase of calibration, that phase leading to a much higher precision.

UNCLASSIFIED

UNCLASSIFIED

is due in part to the limited precision of measurement used. The report describes the work done prior to the second phase of calibration, that phase leading to a much higher precision.

UNCLASSIFIED

UNCLASSIFIED

is due in part to the limited precision of measurement used. The report describes the work done prior to the second phase of calibration, that phase leading to a much higher precision.

UNCLASSIFIED